Nanoscale

Accepted Manuscript

This article can be cited before page numbers have been issued, to do this please use: G. Gong, S. Gao, Z. Xie, X. Ye, Y. Lu, H. Yang, X. Zhu and R. Li, *Nanoscale*, 2020, DOI: 10.1039/D0NR07297D.

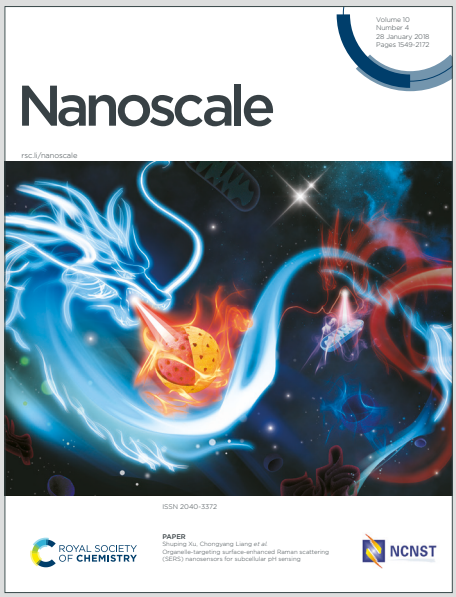

ROYAL SOCIETY OF CHEMISTRY

rsc.li/nanoscale

View Article Online
DOI: 10.1039/D0NR07297D

A visible light-triggered artificial photonic nociceptor with adaptive tunability of threshold

Guodong Gong,[a,b,c] Shuang Gao,*[a,b] Zhuolin Xie,[a,b,c] Xiaoyu Ye,[a,b,c] Ying Lu,[a,b,c] Huali Yang,[a,b] Xiaojian Zhu,[a,b] and Run-Wei Li*[a,b]

[a]*CAS Key Laboratory of Magnetic Materials and Devices, Ningbo Institute of Materials Technology and Engineering, Chinese Academy of Sciences, Ningbo 315201, P. R. China. E-mail: gaoshuang@nimte.ac.cn, runweili@nimte.ac.cn*

[b]*Zhejiang Province Key Laboratory of Magnetic Materials and Application Technology, Ningbo Institute of Materials Technology and Engineering, Chinese Academy of Sciences, Ningbo 315201, P. R. China*

[c]*College of Materials Science and Opto-Electronic Technology, University of Chinese Academy of Sciences, Beijing 100049, P. R. China*

View Article Online
DOI: 10.1039/D0NR07297D

Abstract: An artificial photonic nociceptor that can faithfully emulate the activation of the human visual nociceptive pathway is highly desired for developing advanced intelligent optoelectronic information processing systems. However, the realization of such an artificial device needs sophisticated materials design and is pending to date. Herein, we demonstrate a visible light-triggered artificial nociceptor, composed of the simple ITO/CeO_{2-x}/Pt sandwich structure, that can well reproduce the pain-perceptual characteristics of the human visual system. The abundant oxygen vacancies in the CeO_{2-x} layer account for visible light activation, and the notable built-in electric field due to work function difference of the two electrodes enables the device to work even in a self-powered mode. Key nociceptive characteristics, including threshold, no adaptation, relaxation, and sensitization, are realized in the device, which are attributed to the oxygen vacancy-associated electron trapping and detrapping processes within the CeO_{2-x} layer. More importantly, the threshold light intensity to activate the device can be readily manipulated using a sub-1 V external voltage, resembling the ambient luminance-dependent tunability of threshold of the human visual system. This work opens up a new avenue towards the development of next-generation intelligent and low-power perceptual systems, such as visual prostheses, artificial eyes, and humanoid robots.

Keywords: bioelectronic nanodevice, photonic nociceptor, visible light, tunable threshold, electron trapping/detrapping

View Article Online
DOI: 10.1039/D0NR07297D

1. Introduction

The pain-perceptual ability of nociceptors in the human body is essential to the survival and wellbeing of human beings when interacting with the environment.[1,2] Specifically, nociceptors can perceive precisely and respond appropriately to the potential threating or noxious stimuli, such as extreme heat, intense stress and toxic chemicals.[1-5] Usually, nociceptors are only activated when the external stimulation intensity exceeds a certain threshold value, i.e., responding selectively to the stimuli that are strong enough. Moreover, nociceptors will experience a tonic activation with little or no decay in the response potential amplitude if a constant external arousal is kept up (i.e., no adaptation).[6-8] Plastic modifications, often in the form of relaxation and sensitization, can be further provoked in the nociceptive pathways when the injurious stimuli are intense or prolonged. The relaxation behavior means that nociceptors will exhibit an exaggerated and continual activation even after the removal of injurious stimuli, giving rise to an uncomfortable painful memory track. During the sensitization phase, the threshold value for nociceptor activation decreases (a process known as allodynia) and the nociceptor responds more strongly than in the normal state (a process known as hyperalgesia).[2,9] These key characteristics allow nociceptors to be the frontline in human bodies to defend the potential threats from the environment that may lead to damages.

Recently, the implementation of various nociceptive characteristics in hardware using emerging nanoelectronic devices has attracted tremendous attention for its fascinating applications in next-generation intelligent perceptual systems.[5-8,10-13] For instance, an artificial electronic nociceptor based on a diffusive memristor was designed to establish a

View Article Online
DOI: 10.1039/D0NR07297D

thermal nociceptive system by combining with a thermoelectric module, which is triggered at a temperature close to the threshold of human thermal nociceptors.[7,14] An ultraviolet (UV) damage-sensing nociceptor was also constructed recently based on wide-bandgap metal oxides for future bionic applications.[8] Nevertheless, it is the visible light, instead of UV, that reaches at the retina for human visual perception, but excessive exposure to it can result in tissue damages.[15-19] To prevent the human visual system from being hurt by bright visible light, the ophthalmic nociceptive pathway plays a crucial role, as schematically shown in Fig. 1a. Bright visible light can generally activate the photonic nociceptor in the human visual system and induce protective reflexes such as eyelid closure and pupil contraction through the firing of action potentials.[15,19-22] More importantly, both the incident light intensity and the ambient luminance have contributions to the light-induced activation of the ophthalmic nociceptive pathway.[15,23,24] Under the same ambient luminance, the activation of the photonic nociceptor in the human eyes is only dependent on the incident light intensity. The nociceptor will keep silent if the incident light is below the threshold (the middle panel in Fig. 1a), whereas an action potential will be generated and relayed to the specific spinal cord neurons for the overthreshold stimuli (the top panel in Fig. 1a). On the other hand, the photonic nociceptor in the human eyes is found to show an adaptive threshold adjustment according to the variation of ambient luminance.[15,23,24] Specifically, it can be triggered by a relatively lower and higher incident light intensity in the dark and bright environment, respectively (the middle and bottom panels in Fig. 1a). Transferring such pain-perceptual abilities and particularly the adaptive threshold characteristic into an optoelectronic

View Article Online
DOI: 10.1039/D0NR07297D

implementation will undoubtedly be a huge step towards designing high-performance neuromorphic visual systems in future.

In this study, we demonstrate an energy-efficient artificial photonic nociceptor having a simple "electrode/dielectric/electrode" sandwich structure that can faithfully emulate the activation of the human visual nociceptive pathway. The design principles for such an artificial device are shown in Fig. 1b-1f, which include the following aspects: (i) There are rich in-gap defect states with a relatively wide energy level distribution in the dielectric layer, which not only enable device activation by the entire visible spectrum but also participate in the dynamic trapping and detrapping processes of the photogenerated free electrons to emulate the key characteristics of biological nociceptors;[25,26] (ii) At least one electrode is transparent in the whole visible wavelength region, and the introduction of a clear work function (WF) difference between the two electrodes can induce a notable built-in electric filed in the dielectric layer, permitting spontaneous separation of the photogenerated free electrons and thus self-powered operation of the device;[27-29] (iii) An external electric field can be used to modulate the strength of the built-in electric filed and consequently the photonic nociceptive characteristics of the device. Following these principles, a paradigmatic device composed of the indium-tin oxide/oxygen-deficient cerium dioxide/Pt (ITO/CeO_{2-x}/Pt) sandwich structure is developed. The presence of abundant oxygen vacancies in the CeO_{2-x} layer accounts for visible light activation, and the clear WF difference of ~0.8 eV between the transparent ITO electrode and the high-WF Pt electrode makes the device feasible to work even in a self-powered mode. Owing to the oxygen vacancy-associated electron trapping and detrapping processes in the CeO_{2-x} layer upon light illumination, all

View Article Online
DOI: 10.1039/D0NR07297D

specific nociceptive characteristics, including threshold, no adaptation, relaxation, and sensitization, have been reproduced in the artificial photonic nociceptor. More importantly, the threshold light intensity to activate the device can be effectively modulated by applying a sub-1 V external voltage, making it capable of mimicking the ambient luminance-dependent adaptive threshold characteristic of the human visual system. This work is expected to contribute to the development of future high-performance intelligent and low-power sensing systems, such as visual prostheses, artificial eyes, and humanoid robots.

2. Results and discussion

Fig. 2a shows a cross-sectional transmission electron microscope (TEM) image of the fabricated photonic nociceptor, which constitutes a ~25 nm CeO_{2-x} layer sandwiched between a pair of top ITO and bottom Pt electrodes. The CeO_{2-x} layer is polycrystalline and has a smooth surface with the roughness of only ~1.79 nm (Fig. S1-S2). The selection of CeO_{2-x} as the dielectric layer is due to its fluorite crystalline structure with rich defect energy levels in the bandgap, which can not only extend the photoresponsive window from the UV to the entire visible region but also provide effective trapping sites for the photogenerated free electrons[25,26]. Such hypothesis has been confirmed by X-ray photoelectron spectroscopy (XPS) and UV-Visible absorption spectrum analysis. Specifically, the characteristic peak for oxygen deficiencies/vacancies (O_D) at ~530.9 eV is observed in the O 1s spectrum, in addition to the characteristic peaks corresponding to the expected lattice oxygens (O_L) and surface absorbed oxygens (O_A) locating at ~529.2 eV and ~533.0 eV, respectively (Fig. 2b).[30,31] Based on the fitting results, the area percentages of O_D and O_L in the whole spectrum are 38.4% and 51.3%, respectively, thus leading to a high O_D percentage of 42.8%

View Article Online
DOI: 10.1039/D0NR07297D

(= 38.4%/(38.4% + 51.3%)) in the film. Accordingly, for the Ce 3d spectrum in Fig. 2c, one can see not only the peaks for Ce^{4+} ions at 898.0 eV (V‴) and 916.5 eV (U‴) but also the peak for Ce^{3+} ions at 884.0 eV (V′).[25,30,32,33] The two points accord well with each other and demonstrate definitely that there exist a large number of oxygen vacancies in the as-prepared CeO_{2-x} thin film. Due to the rich in-gap defect energy levels caused by these vacancies, clear absorption over the entire visible region of 400-700 nm is indeed realized in the CeO_{2-x} film, as shown in Fig. 2d. For the electrodes, ITO is a typical transparent conducting material with a relatively low WF of ~4.8 eV,[34] whereas Pt is a commonly used inert metal electrode with a very high WF of ~5.6 eV.[35] As such, a large WF difference of up to ~0.8 eV can be obtained, which can generate a notable built-in electric field in the device. This field can lead to spontaneous separation of the photogenerated free electrons and thus make the device feasible to work even in a self-powered mode that is highly promising for low-power electronics.[27-29,34]

The basic photoresponsive properties of the ITO/CeO_{2-x}/Pt device and their correspondence to the characteristics of a biological photonic nociceptor are firstly discussed. Fig. 3a-3c show the pain-perceptual threshold behaviors of the device in the self-powered mode using blue, green, and red optical irradiations, respectively. Taking Fig. 3b as the example, green light pulses having a width of 3.6 s and an intensity that gradually increases from 0.5 to 5 pW/μm^2 were successively applied to the device to emulate the external stimuli (upper panel), and the photocurrent representing the response signal of the artificial photonic nociceptor was simultaneously recorded (bottom panel). One can see that the photocurrent is negligible when the light intensity is below 1.2 pW/μm^2 (highlighted by the black dotted line).

View Article Online
DOI: 10.1039/D0NR07297D

Moreover, further increase of the light intensity to 5 pW/μm^2 can result in a larger photocurrent output. As such, the device can successfully emulate the "threshold" characteristic of a biological photonic nociceptor, where a 1.2 pW/μm^2 threshold is estimated for the green light irradiation (i.e., T_G = 1.2 pW/μm^2). It is worth mentioning herein that such a threshold matches very well with the discomfort threshold of ~1-2 pW/μm^2 in the human eyes induced by the visible light.[19,36-38] Similarly, the pain-perceptual thresholds of the device for blue and red light irradiations can be estimated to be T_B = 0.4 pW/μm^2 and T_R = 14.5 pW/μm^2, respectively (Fig. 3a and 3c). It is noted that the photonic nociceptor in the human eyes also has a relatively higher and lower sensitivity to the blue and red light, respectively.[20,39] In other words, the most harmful component of the visible light to the human eyes comes from the blue wavelength. The threshold ratio between T_R and T_B of the artificial nociceptor is calculated to be 14.5/0.4 = 36.25, which is very close to the value of ~40 obtained from an photonic nociceptor in the human eyes.[20]

A reasonable explanation for the threshold characteristic of the device can be found in Fig. 1b-1d. Owing to thermal excitation, the shallow oxygen vacancies in the CeO_{2-x} layer become empty and can thus act as the trapping sites for free electrons (Fig. 1b). When an incident optical stimulus is applied to the device, the electrons trapped in the deep oxygen vacancies can be excited into the conduction band and then, driven by the build-in electric field, migrate towards the ITO electrode. If the light intensity is below the threshold, the photogenerated free electrons are less and all of them can be re-trapped by the rich empty trapping sites, thus leading to a negligible photocurrent (Fig. 1c). In contrast, all the trapping sites can be filled by the ample free electrons excited by an overthreshold stimulus and the

View Article Online
DOI: 10.1039/D0NR07297D

remaining electrons can therefore migrate into the ITO electrode, resulting in a remarkable photocurrent in the external circuit (Fig. 1d).

Besides operating in the self-powered mode, an external read voltage (V_r) can be applied onto the device to greatly amplify the photoresponsive signal during light illumination and, in particular, the relaxation signal immediately after light illumination (Fig. S3). As such, to better clarify the other nociceptive characteristics of this device, a V_r of 0.4 V is used hereafter except for specific clarification. Photocurrent response of the device (lower panel) to multiple green optical pulses with the intensity of 20 pW/μm^2 (upper panel) is shown in Fig. 3d. It is observed that the photocurrent maintains almost at the same level as the increase in pulse number of the constant noxious stimuli. Similar results can also been found for the device under multiple green optical pulses with the intensities of 5 and 11 pW/μm^2 (Fig. S4). Generally, a dynamic equilibrium can be established between the generating and trapping processes of free electrons after the device is exposed to a specific optical stimulus, thus enabling the device to output an almost invariant photocurrent under a series of identical pulse stimuli. This phenomenon closely resembles the "no adaptation" characteristic of a biological photonic nociceptor, and is essential for the human body to guard against the repeated harmful optical stimuli.

It is emphasized that the painful sensation is not generated by an immutable, hardwired system, but rather achieved by the engagement of highly plastic molecules and circuits.[2,9] As mentioned in the introduction, relaxation and sensitization are the two critical characteristics relating to plastic modifications in the nociceptive pathways. Herein, the relaxation characteristic refers to how the response signal decays over time after the removal of external

View Article Online
DOI: 10.1039/D0NR07297D

stimuli. Such intriguing biological behavior can also be successfully mimicked by our artificial nociceptor. Fig. 4a shows a typical photocurrent evolution process of the ITO/CeO_{2-x}/Pt device under green light exposure with an intensity of 160 pW/μm^2 and an illuminating time of 4 s, followed by a noticeable current decay process of ~25.7 s after the removal of optical irradiation. Such residual current can be attributed to the metastability of the re-trapped free electrons at the shallow trapping sites, which will be gradually detrapped by thermal excitation after the removal of optical irradiation and then migrate into the ITO electrode, as schematically shown in Fig. S5.[6,8] Statistical analysis has been made to better reveal the current decay process as well as the photocurrent response of the device. As illustrated in Fig. 4b, the peak of photocurrent (I_p) gradually increases from ~1.1 to ~30.3 pA as the input optical pulse intensity is changed from 5 to 220 pW/μm^2. The variations of the initial decay current (I_d) and the current decay time (t_d) with the input optical pulse parameters are presented in Fig. 4c and 4d, respectively. Notably, a larger I_d and a longer t_d can be caused by either a higher optical intensity or a longer illuminating time. These resemble the common human experience that the more serious the injury is, the stronger and longer the pain is sensed.

The sensitization characteristic of biological nociceptors can be represented by allodynia and hyperalgesia, referring to the perception of pain elicited by an innocuous stimulus and the increased painful response to a noxious stimulus, respectively.[2,4] They are caused by the release of proinflammatory mediators after the exposure to a damaging or intense stimulus.[2,9] Fig. 5a schematically shows the typical stimuli versus response relationship of a biological nociceptor in normal (no injured) and injured conditions, where the allodynia and

View Article Online
DOI: 10.1039/D0NR07297D

hyperalgesia features are separately indicated by the horizontal and vertical arrows. To emulate the two features, an extremely high green light illumination (110 or 130 pW/μm^2) was applied to the device to induce the injured condition, and two identical subthreshold or small overthreshold optical pulses were used (one just before and the other one just after the damaging illumination) to reveal the effect of injury on device response.[8,12] It is seen from Fig. 5b that, owing to the relaxation process, painful sensation under subthreshold stimuli is detected right after the damaging illumination of 130 pW/μm^2. In other words, the pain-perceptual threshold has been notably decreased in the injured condition. Meanwhile, under the two small overthreshold optical pulses, a significant increase in the photocurrent is obtained after the damaging illumination than that before (Fig. 5c). This can be attributed to the overlap between the response signal induced purely by the later overthreshold stimulus and the relaxation process following the damaging illumination. Fig. 5d shows the dependence of the photocurrent on the illumination intensity for the device in normal and injured states, which resembles the allodynia and hyperalgesia features of a biological nociceptor. Moreover, a more obvious shift in photocurrent response is observed for the higher damaging illumination of 130 pW/μm^2, which is just as expected from our common painful experience. The raw data for this figure can be found in Fig. S6.

Beyond the above normal nociceptive characteristics, there is an exclusive characteristic known as “adaptive threshold” for the photonic nociceptor in the human eyes.[15,23,24] Specifically, the threshold light intensity has a strong dependence on the ambient luminance, and a lower and higher threshold is exhibited by the biological photonic nociceptor in the dark and bright environment, respectively. Such characteristic is crucial for the human eyes

View Article Online
DOI: 10.1039/D0NR07297D

to avoid being hurt in the environments with variable brightness, the optoelectronic implementation of which will thus have great significance in developing visual prostheses and humanoid robotics in future. Interestingly, it is found that the threshold light intensity to activate the ITO/CeO_{2-x}/Pt device can be flexibly modulated by applying a small V_r, as illustrated in Fig. 6a and Fig. S7. For example, a positive V_r of 0.6 V reduces the pain-perceptual threshold from 1.2 to 0.5 pW/μm^2, whereas a negative V_r of –0.45 V can improve it from 1.2 to 11 pW/μm^2. Fig. 6b shows the variation trend of the device's nociceptive threshold with the V_r, clearly suggesting that a relatively lower and higher threshold can be achieved under positive and negative biases, respectively. The large threshold modulation range of over one order of magnitude realized by only changing the V_r within 1 V indicates a high adaptability of the artificial photonic nociceptor for various environments. Such observation can be attributed to the dynamic modulation of the photocurrent efficiency of the device by applying the V_r, as schematically shown in Fig. 1e and 1f. Under a positive V_r, the built-in electric field is strengthened, which can promote the separation and extraction of the photogenerated free electrons and thus leads to a higher photocurrent efficiency that corresponding to a lower threshold. On the contrary, a negative V_r will weaken the built-in electric field and results ultimately in a lower photocurrent efficiency that corresponding to a higher threshold.

Before concluding, a detailed performance comparison between our artificial photonic nociceptor and the previously reported ones is provided in Table 1. It is clear that our ITO/CeO_{2-x}/Pt device has not only a simple structure but also a wide light-responsive region to some extent. More importantly, the threshold current of our device is at least 10^5 times

View Article Online
DOI: 10.1039/D0NR07297D

smaller than that of previously reported artificial photonic nociceptors and the adaptive threshold characteristic is demonstrated for the first time in our device. Also, it deserves to be mentioned that our device works in the pA level, which can be up to ~10^9 times smaller than that of the previously reported diffusive memristor-based electronic nociceptor.[7,14] As such, the ITO/CeO_{2-x}/Pt device should be highly useful in future high-performance intelligent sensing systems, such as visual prostheses, artificial eyes, and humanoid robots. In particular, the unusual ability of self-powered operation, the extremely low threshold current and the high adaptability of threshold under a sub-1 V external voltage could promise the device a less power consumption and a wider applicability. If we use light to encode the sensor output signals for heat, pressure, and so on, the device could been further employed to construct various optically interconnected nociceptive systems with highly enhanced operating speed and signal bandwidth. Moreover, the structure and working mechanism of the device could be readily adapted to develop flexible organic nociceptors that are highly desired in future intelligent wearable electronic systems such as electronic skin.

3. Conclusion

In summary, we propose and demonstrate a visible light-triggered artificial photonic nociceptor composed of the simple ITO/CeO_{2-x}/Pt sandwich structure, which can well mimic the intelligent nociceptive characteristics including threshold, no adaptation, relaxation, and sensitization of its biological counterpart under light illumination. In particular, the threshold light intensity and threshold ratio between T_R and T_B of the artificial nociceptor are quantitatively comparable with those of a biological photonic nociceptor in the human eyes. More importantly, the threshold light intensity to activate the artificial nociceptor can be

View Article Online
DOI: 10.1039/D0NR07297D

flexibly manipulated by a sub-1 V external voltage, making the device highly suitable for the mimicry of ambient luminance-dependent adaptive tunability of threshold of the human visual system. This proof-of-concept device can contribute to the development of future high-performance intelligent and low-power sensing systems, such as visual prostheses, artificial eyes, and humanoid robots.

4. Experimental

4.1 Device Fabrication

The polycrystalline CeO_{2-x} thin film with the thickness of ~25 nm was firstly deposited on a commercially available Pt/Ti/SiO_2/Si substrate (1 cm × 1 cm) by radio-frequency (RF) magnetron sputtering technique using a CeO_2 ceramic target at room temperature. During the deposition process, the RF power, chamber pressure, and Ar/O_2 ratio were fixed at 60 W, 1 Pa, and 1:2, respectively. Then, the transparent conducting ITO electrodes, with a diameter of 150 μm and a thickness of ~100 nm, were deposited by pulsed laser deposition (PLD) technique at room temperature through a metal shadow mask. The detailed PLD growing parameters were 248 nm laser wavelength, 78 mJ laser energy, 1 Hz pulse frequency, and 0.8 Pa oxygen pressure.

4.2 Device Characterization

Crystalline structure and surface morphology of the as-deposited CeO_{2-x} thin film were characterized by X-ray diffraction (XRD, Bruker AXS, D8 Discover) with the Cu Kα radiation and scanning probe microscope (SPM, Veeco Dimension 3100V), respectively. Chemical composition and optical absorption property of the CeO_{2-x} thin film were analyzed by XPS (Shimadzu, AXIS ULTRA DLD) and UV-Visible spectrometer (Perkin Elmer,

View Article Online
DOI: 10.1039/D0NR07297D

Lambda 950), respectively. After calibrating the binding energies by referring to the C 1s hydrocarbon peak at 284.6 eV, background correction and peak fitting of the obtained XPS data were performed using the CASA XPS software. For the absorbance of the CeO_{2-x} thin film, it was obtained by firstly measuring the absorbance of the individual CeO_{2-x}/Pt and pure Pt samples and then subtracting the absorbance of the pure Pt sample from that of the CeO_{2-x}/Pt sample. The cross-sectional specimen was fabricated using a focused ion beam (FIB) system (FEI Helios 450S) and then examined by a FEI TEM (Titan Themis 200). All the photoresponsive current–voltage (*I–V*) behaviors of the device were measured on a Lakeshore probe station using a precision semiconductor parameter analyzer (Keithley 4200). The directions of positive read voltage and photocurrent were defined to be from the ITO to the Pt electrode. Commercially available light-emitting diodes (LEDs) with red (630 nm), green (528 nm), and blue (459 nm) emissions were used as the light sources. The detailed light spectra of LEDs and device measurement configuration can be found in our previous work,[41] and the illuminating intensities were calibrated by a light meter (Li-250A, LI-COR). To exclude the influence of the ambient light, all the photoresponsive measurements were conducted in the dark chamber of the probe station.

Conflicts of interest

There are no conflicts to declare.

Acknowledgements

This work was supported by the National Key R&D Program of China (2017YFB0405604), National Natural Science Foundation of China (61704178,

View Article Online
DOI: 10.1039/D0NR07297D

61974179, 61841404, 51525103, and 51931011), Youth Innovation Promotion Association of the CAS (2020297), Natural Science Foundation of Zhejiang Province (LR17E020001), and Ningbo Natural Science Foundation (202003N4029).

References

1 C. J. Woolf and Q. Ma, *Neuron*, 2007, **55**, 353-364.

2 A. I. Basbaum, D. M. Bautista, G. Scherrer and D. Julius, *Cell*, 2009, **139**, 267-284.

3 D. Julius and A. I. Basbaum, *Nature*, 2001, **413**, 203-210.

4 A. E. Dubin and A. Patapoutian, *J. Clin. Invest.*, 2010, **120**, 3760-3772.

5 G. Feng, J. Jiang, Y. Zhao, S. Wang, B. Liu, K. Yin, D. Niu, X. Li, Y. Chen, H. Duan, J. Yang, J. He, Y. Gao and Q. Wan, *Adv. Mater.*, 2020, **32**, 1906171.

6 Y. Kim, Y. J. Kwon, D. E. Kwon, K. J. Yoon, J. H. Yoon, S. Yoo, H. J. Kim, T. H. Park, J. W. Han, K. M. Kim and C. S. Hwang, *Adv. Mater.*, 2018, **30**, 1704320.

7 J. H. Yoon, Z. Wang, K. M. Kim, H. Wu, V. Ravichandran, Q. Xia, C. S. Hwang and J. J. Yang, *Nat. Commun.*, 2018, **9**, 417.

8 M. Kumar, H. S. Kim and J. Kim, *Adv. Mater.*, 2019, **31**, 1900021.

9 M. C. Pace, M. B. Passavanti, L. D. Nardis, F. Bosco, P. Sansone, V. Pota, M. Barbarisi, A. Palagiano, F. A. Iannotti, E. Panza and C. Aurilio, *J. Cell. Physiol.*, 2018, **233**, 2824-2838.

10 M. Xiao, D. Shen, M. H. Futscher, B. Ehrler, K. P. Musselman, W. W. Duley and Y. N. Zhou, *Adv. Electron. Mater.*, 2020, **6**, 1900595.

11 J. Ge, S. Zhang, Z. Liu, Z. Xie and S. Pan, *Nanoscale*, 2019, **11**, 6591-6601.

12 L. Zhou, S. R. Zhang, J. Q. Yang, J. Y. Mao, Y. Ren, H. Shan, Z. Xu, Y. Zhou and S. T. Han, *Nanoscale*, 2020, **12**, 1484-1494.

13 M. K. Akbari, J. Hu, F. Verpoort, H. Lu and S. Zhuiykov, *Nano-Micro Lett.*, 2020, **12**, 1-16.

14 Y. Sun, C. Song, S. Yin, L. Qiao, Q. Wan, R. Wang F. Zeng and F. Pan, *Adv. Electron. Mater.*, 2020, DOI: 10.1002/aelm.202000695.

15 M. Różanowska and T. Sarna, *Photochem. Photobiol.*, 2005, **81**, 1305-1330.

16 D. H. Sliney, *Int. J. Toxicol.*, 2002, **21**, 501-509.

17 E. A. Boettner and J. R. Wolter, *Invest. Ophthalmol. Vis. Sci.*, 1962, **1**, 776-783.

18 D. H. Sliney, *J. Photochem. Photobiol. B-Biol.*, 2001, **64**, 166-175.

19 K. Okamoto, A. Tashiro, Z. Chang and D. A. Bereiter, *Pain*, 2010, **149**, 235-242.

20 S. Lei, H. C. Goltz, X. Chen, M. Zivcevska and A. M. Wong, *Invest. Ophthalmol. Vis. Sci.*, 2017, **58**, 1449-1454.

21 J. J. Hunter, J. I. Morgan, W. H. Merigan, D. H. Sliney, J. R. Sparrow and D. R. Williams, *Prog. Retin. Eye Res.*, 2012, **31**, 28-42.

22 S. Dolgonos, H. Ayyala and C. Evinger, *Invest. Ophthalmol. Vis. Sci.*, 2011, **52**, 7852-7858.

23 F. Li, W. Cao and R. E. Anderson, *Exp. Eye Res.*, 2001, **73**, 569-577.

24 F. Li, W. Cao and R. E. Anderson, *Invest. Ophthalmol. Vis. Sci.*, 2003, **44**, 4968-4975.

25 H. Tan, G. Liu, X. Zhu, H. Yang, B. Chen, X. Chen, J. Shang, W. D. Lu, Y. Wu and R. W. Li, *Adv. Mater.*, 2015, **27**, 2797-2803.

26 H. Tan, G. Liu, H. Yang, X. Yi, L. Pan, J. Shang, S. Long, M. Liu, Y. Wu and R. W. Li, *ACS Nano*, 2017, **11**, 11298-11305.

27 L. Su, W. Yang, J. Cai, H. Chen and X. Fang, *Small*, 2017, **13**, 1701687.

28 S. M. Hatch, J. Briscoe and S. Dunn, *Adv. Mater.*, 2013, **25**, 867-871.

29 L. Peng, L. Hu and X. Fang, *Adv. Funct. Mater.*, 2014, **24**, 2591-2610.

30 A. Younis, D. Chu and S. Li, *J. Phys. D: Appl. Phys.*, 2012, **45**, 355101.

31 H. Xu, D. H. Kim, Z. Xiahou, Y. Li, M. Zhu, B. Lee and C. Liu, *J. Alloys Compd.*, 2016, **658**, 806-812.

32 Y. W. Zhang, R. Si, C. S. Liao, C. H. Yan, C. X. Xiao and Y. Kou, *J. Phys. Chem. B*, 2003, **107**, 10159-10167.

33 D. Chu, Y. Masuda, T. Ohji and K. Kato, *Phys. Status. Solidi. A*, 2012, **209**, 139-142.

34 S. Gao, C. Song, C. Chen, F. Zeng and F. Pan, *J. Phys. Chem. C*, 2012, **116**, 17955-17959.

35 J. H. Yoon, D. E. Kwon, Y. Kim, Y. J. Kwon, K. J. Yoon, T. H. Park, X. L. Shao and C. S. Hwang, *Nanoscale*, 2017, **9**, 11920-11928.

36 P. A. Kowacs, E. J. Piovesan, L. C. Werneck, C. E. Tatsui, M. C. Lange, L. C. Ribas and H. P. Silva, *Cephalalgia*, 2001, **21**, 184-188.

37 A. Woodhouse and P. D. Drummond, *Cephalalgia*, 1993, **13**, 417-421.

38 S. M. Sykes, W. G. Robison, M. Waxler and T. Kuwabara, *Invest. Ophthalmol. Vis. Sci.*, 1981, **20**, 425-434.

View Article Online
DOI: 10.1039/D0NR07297D

39 J. Vicente-Tejedor, M. Marchena, L. Ramírez, D. García-Ayuso, V. Gómez-Vicente, C. Sánchez-Ramos, P. Villa and F. Germain, *Plos One*, 2018, **13**, e0194218.

40 H. Xu, M. K. Akbari, F. Verpoort and S. Zhuiykov, *Nanoscale*, 2020, **12**, 20177-20188.

41 S. Gao, G. Liu, H. Yang, C. Hu, Q. Chen, G. Gong, W. Xue, X. Yi, J. Shang and R. W. Li, *ACS Nano*, 2019, **13**, 2634-2642.

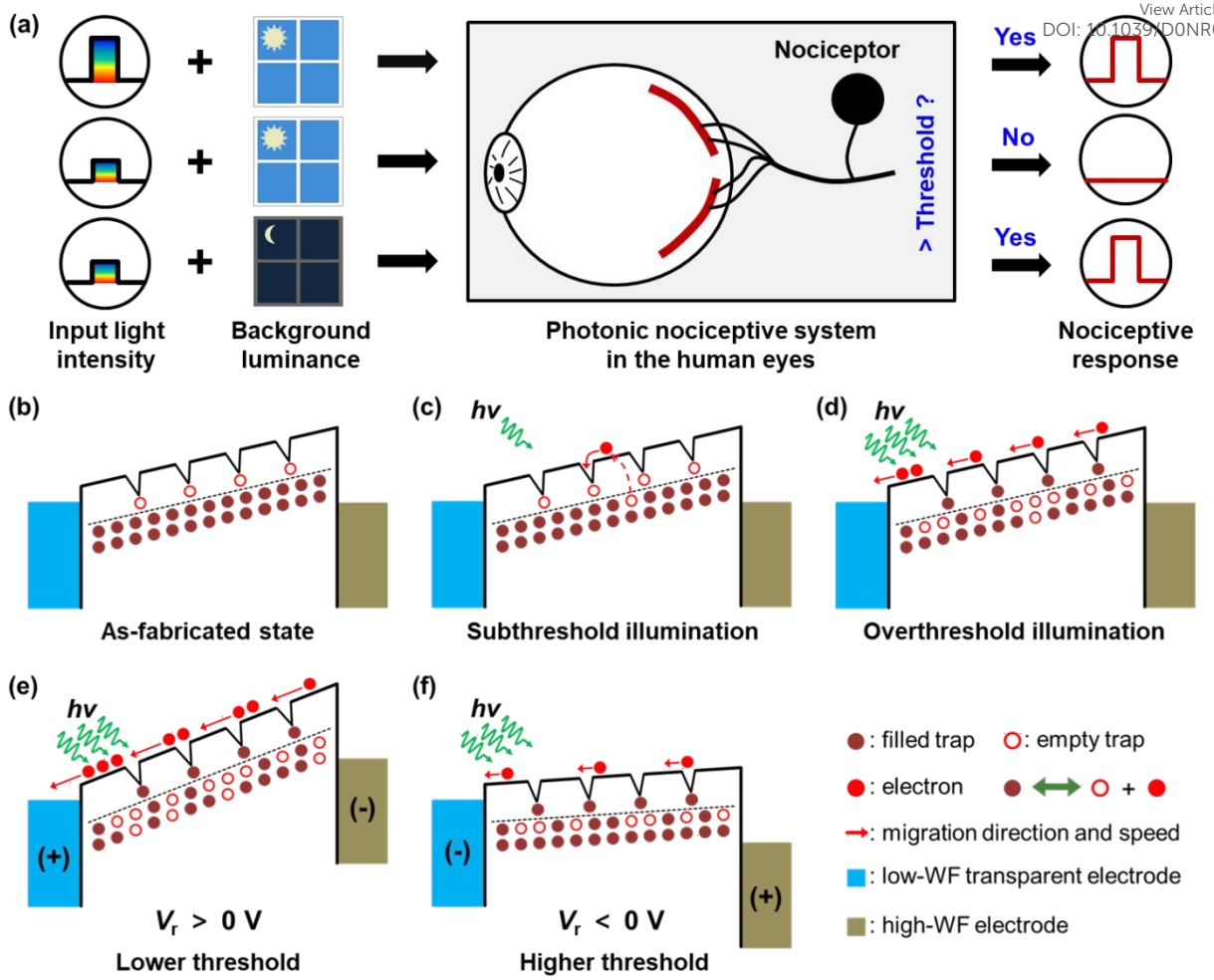

Fig. 1 Working principle of the photonic nociceptive system in the human eyes and the design principles for a visible light-triggered artificial photonic nociceptor. (a) Schematic illustration of light-induced activation of the ophthalmic nociceptive pathway, depending on both the incident light intensity and the ambient luminance. (b-d) Schematic band diagrams of the proposed artificial photonic nociceptor in the as-fabricated state, under subthreshold light illumination, and under overthreshold light illumination, respectively. (e,f) Schematic modulation mechanism of the artificial photonic nociceptor's threshold by applying various external voltages. A relatively lower and higher threshold is achieved under positive and negative biases, respectively.

View Article Online
DOI: 10.1039/D0NR07297D

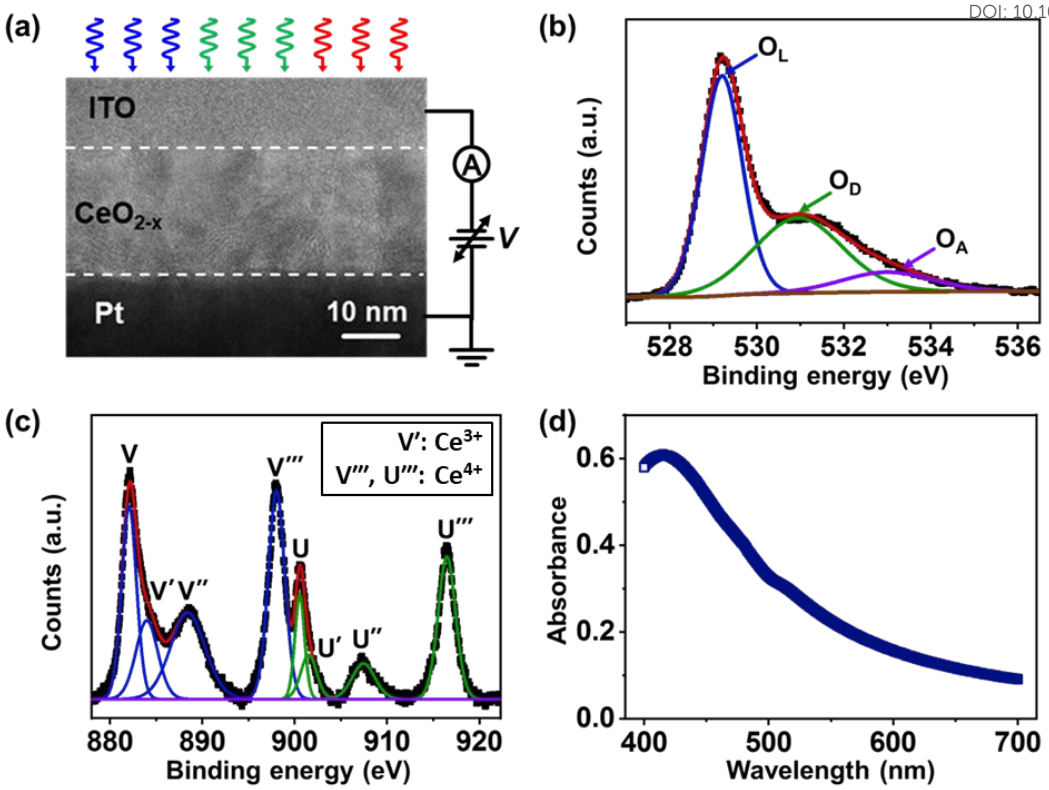

Fig. 2 Device characterization of the fabricated ITO/CeO_{2-x}/Pt artificial photonic nociceptor. (a) Cross-sectional TEM image of the device, accompanied by the measurement configuration for photoelectric characteristics. (b) Core-level O 1s XPS spectra of the CeO_{2-x} thin film. (c) Core-level Ce 3d XPS spectra of the CeO_{2-x} thin film. The peaks at 882.1 eV (V), 884.0 eV (V′), 888.4 eV (V″), and 898.0 eV (V‴) can be ascribed to the components of Ce $3d_{5/2}$, while the peaks at 900.5 eV (U), 901.5 eV (U′), 907.5 eV (U″), and 916.5 eV (U‴) are attributed to the components of Ce $3d_{3/2}$. (d) UV-Visible absorption spectrum of the CeO_{2-x} thin film in the visible region.

View Article Online
DOI: 10.1039/D0NR07297D

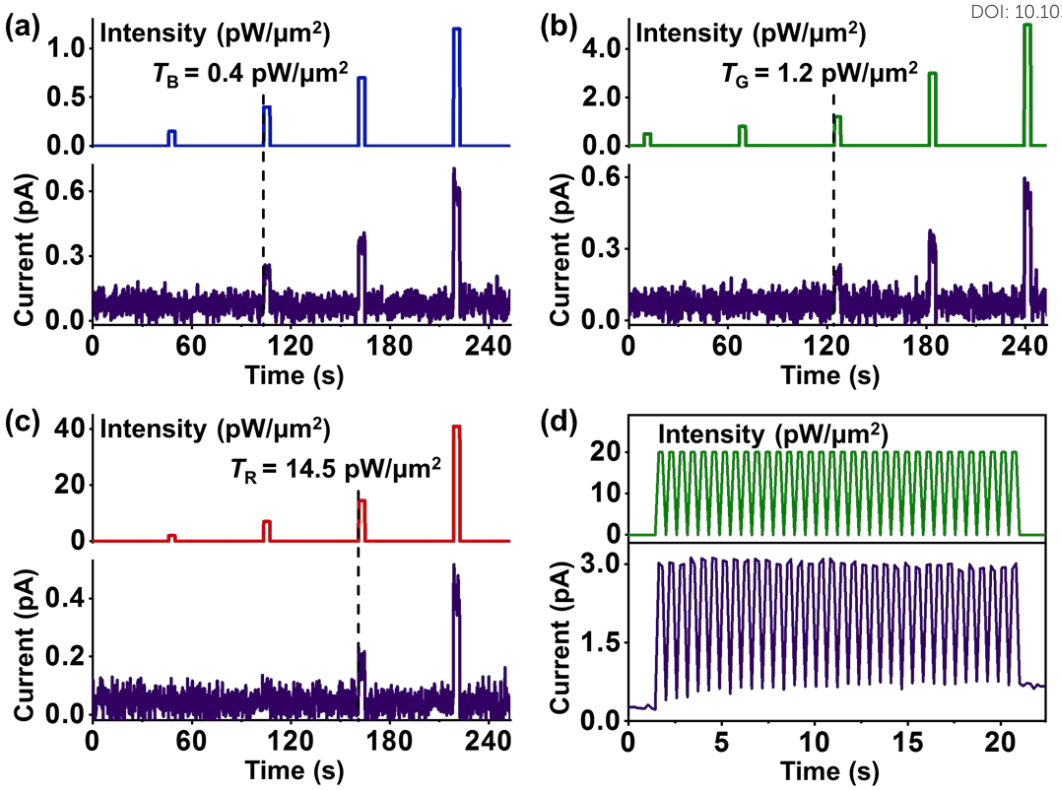

Fig. 3 Photonic threshold and no adaptation characteristics of the ITO/CeO_{2-x}/Pt device. Intensity-dependent photocurrent response of the device in self-powered mode using (a) blue, (b) green and (c) red optical irradiation. Pulse width, 3.6 s. (d) Photocurrent response of the device to multiple green optical pulses with the intensity of 20 pW/μm². Pulse width, 0.2 s.

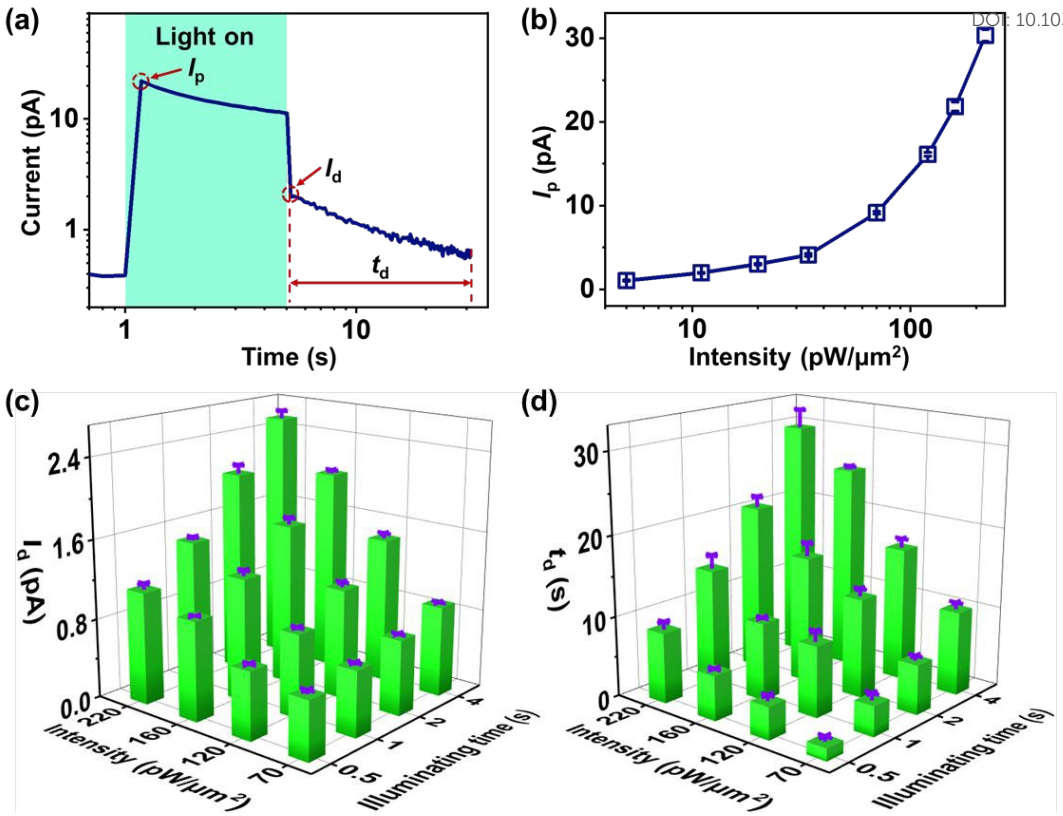

Fig. 4 Photonic relaxation characteristics of the ITO/CeO_{2-x}/Pt device under green light illumination. (a) Typical photocurrent evolution process of the device. Light intensity, 160 pW/μm^2; pulse width, 4 s. (b) The relationship between the I_p and the optical intensity. (c,d) The variations of I_d and t_d with the input optical pulse parameters.

View Article Online
DOI: 10.1039/D0NR07297D

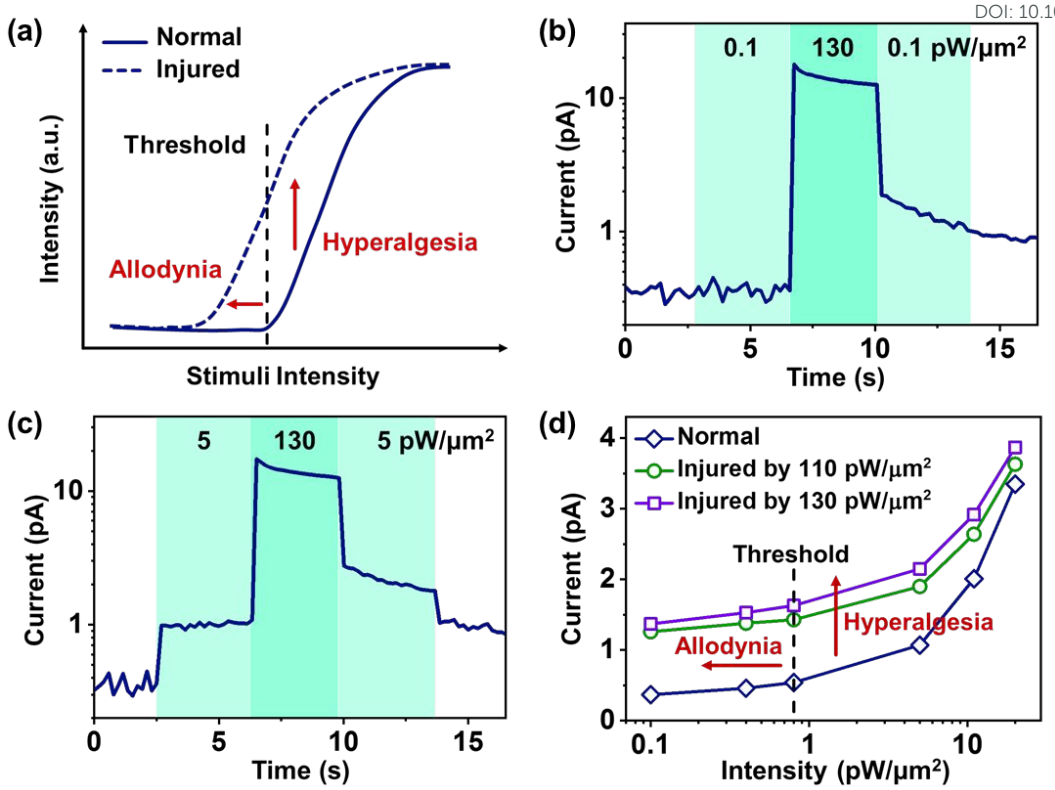

Fig. 5 Photonic allodynia and hyperalgesia characteristics of the ITO/CeO_{2-x}/Pt device under green light illumination. (a) Typical stimuli versus response relationship of the biological nociceptor in normal and injured conditions. (b) A relatively smaller threshold can be achieved after the damaging illumination. (c) The photocurrent response increases significantly after the damaging illumination. (d) Photocurrent response properties of the device in normal and injured conditions. Damaging illumination intensity, 110 or 130 pW/μm^2; pulse width, 3.5 s.

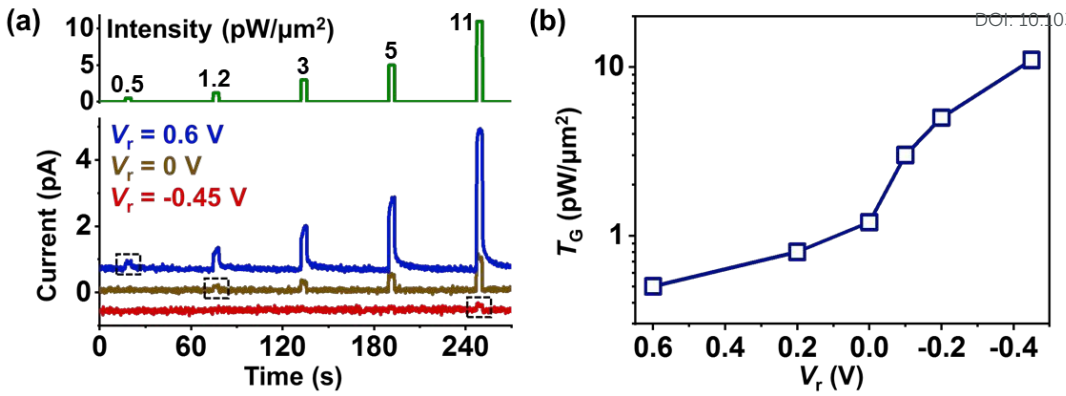

Fig. 6 Threshold modulation of the ITO/CeO_{2-x}/Pt device by applying various external voltages. (a) Photocurrent response of the device under different read voltages. The black dotted squares highlight the response thresholds. (b) Nociceptive threshold of the device as a function of the read voltage. Light color, green; pulse width, 3.6 s; light intensity, 0.5 to 11 pW/μm².

View Article Online
DOI: 10.1039/D0NR07297D

Table 1. Comparison between previously reported photonic nociceptors and this work. Symbols " √ " and "-" denote demonstrated and non-demonstrated nociceptive functions, respectively. UV: ultraviolet; Vis: visible region; *R*: red; *G*: green; *B*: blue.

Device structure	Light source	Threshold light intensity (mW/cm^2)	Threshold current (μA)	No adaptation	Relaxation	Sensitization	Adaptive threshold
ZnO/ATO/FTO[8]	UV	9.5	0.3	√	√	√	-
ITO/PMMA:Azo-Au NPs/Al[12]	UV	40	20	-	√	√	-
ITO/TiO_2/Ga_2O_3(Ar)/Au[13]	UV	15	0.02	√	√	√	-
ITO/TiO_2/Ga_2O_3(N_2)/Au[40]	Vis	0.005 (*R*)	0.02	√	√	√	-
ITO/CeO_{2-x}/Pt (this work)	Vis	0.04 (*B*) 0.12 (*G*) 1.45 (*R*)	2×10^{-7}	√	√	√	√

View Article Online
DOI: 10.1039/D0NR07297D

Graphical Table of Contents:

An energy-efficient visible light-triggered artificial photonic nociceptor is demonstrated, which opens up a new avenue towards the development of next-generation intelligent and low-power perceptual systems, such as visual prostheses and humanoid robots.